RSC Advances

ROYAL SOCIETY OF CHEMISTRY

www.rsc.org/advances

Graphical abstract

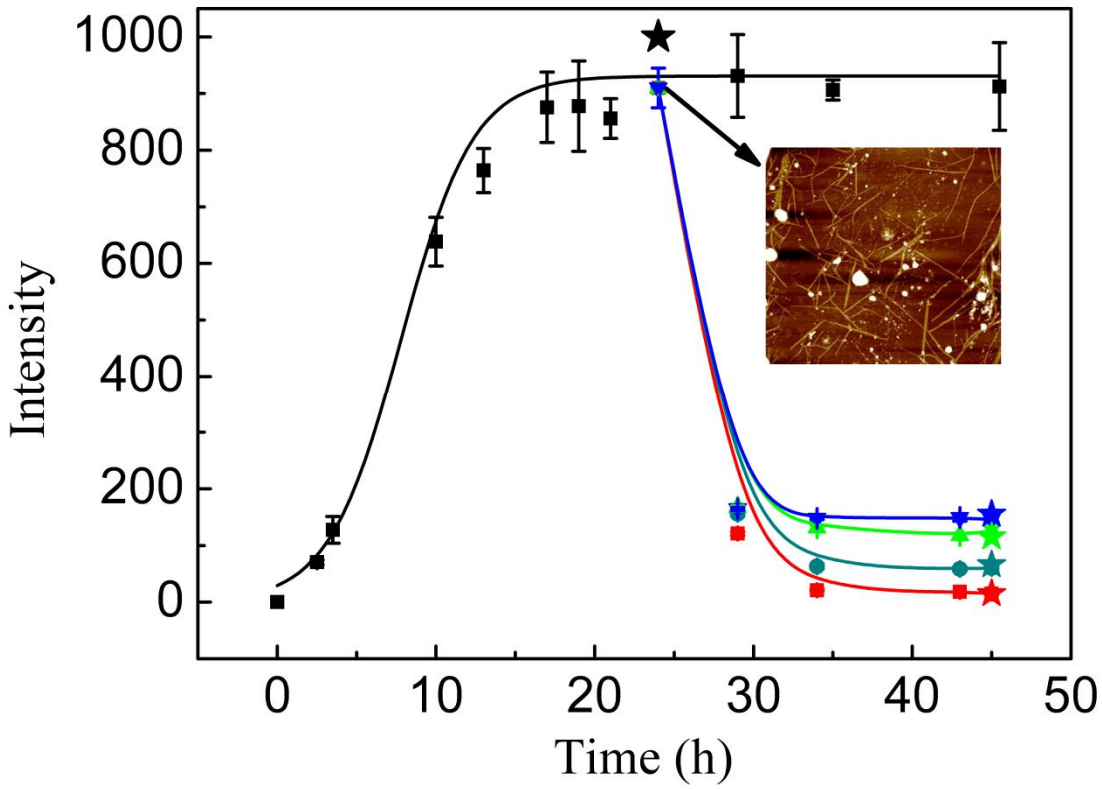

Structural characteristics of (–)-epigallocatechin-3-gallate inhibiting amyloid Aβ42 aggregation and remodeling amyloid fibers

Yun Liu[1], Yang Liu[#1], Shihui Wang[#1], Shengzhao Dong[#1], Ping Chang[2], Zhaofeng Jiang[2]

[1] Beijing Key Laboratory of Bioprocess, College of Life Science and Technology, Beijing University of Chemical Technology, Beijing 100029 China;

[2] College of Applied Arts and Science, Beijing Union University, Beijing 100101 China

# Equal contributor

* Correspondence author: Yun Liu

Tel: +86 -10-64421335; Fax: +86 -10-64416428;

E-mail address: liuyun@mail.buct.edu.cn or liuyunprivate@sina.com

ABSTRACT

To elucidate the structural requirements by which EGCG analogs inhibit Aβ42 protein aggregation and remodel amyloid fibers, the molecular interactions between Aβ42 and four EGCG analogs, epigallocatechin-3-gallate (EGCG), (–)-gallocatechin gallate (GCG), (–)-epicatechin-3-gallate (ECG) and (–)-epigallocatechin (EGC), were investigated by thioflavin T fluorescence (ThT), circular dichroism (CD), atomic force microscope (AFM), differential scanning calorimeter (DSC) and BCA protein assay. Results revealed that the four EGCG analogs had abilities of preventing the increase of β-sheet contents and inhibiting Aβ42 fibrillation when added in the lag and growth phases of Aβ42 fibrillation process. When added in the equilibrium phase, the four EGCG analogs can disaggregate the preformed protofibrils/fibrils to oligomers and unfold or partially unfold oligomers. It was also observed that EGCG showed the highest inhibitory effect on Aβ42 fibrillation, followed by GCG, ECG and EGC. From the values of IC_{50}, kinetic parameters, secondary structures, thermo-stability and solubility measurement, a reasonable conclusion can be preliminarily drawn that the structural contribution efficiency of EGCG to inhibit Aβ42 aggregation and remodel Aβ42 amyloid fibrils decreases by the order of 3'-hydroxyl group of trihydroxyphenyl ring > gallol ester moiety > stereoisomer. The findings in this work provide the structure based molecular interaction mechanism between EGCG analogs and Aβ42 amyloid protein.

***Keywords*:** Aβ42 protein; EGCG analogs; Fibrillation/Aggregation; Remodel

Introduction

The typical feature of Alzheimer's disease (AD) is the aggregation of amyloid β-protein (Aβ) from soluble random-coil into β-sheet rich fibrils [1]. Aβ protein contains several different species (Aβ39-43) according to the numbers of amino acids in the backbone structure. Among them, amyloid β-protein 42 (Aβ42) has been considered as the most crucial factor for the onset of AD due to its extremely severe neurotoxicity and strong aggregation capability [2, 3]. Hence, prevention of Aβ42 aggregation has a key point to AD pathology [4]. Researchers have revealed that (−)-epigallocatechin 3-gallate (EGCG) shows excellent inhibitory effect for the aggregation/fibrillation of Aβ protein both *in vivo* and *in vitro* [5-7]. For instance, Porat and co-workers addressed that EGCG was a potent inhibitor of Aβ40 aggregation and its IC_{50} was 3.0 μM [8]. EGCG is thought to bind to unaggregated polypeptides and redirect the pathway of amyloid formation to off-pathway nontoxic oligomers [9], and it is a promising new drug-delivery system to the special position [10]. Wang and co-workers [11] reported that there were no specific interactions and binding sites in the Aβ42 and EGCG binding from the data of isothermal titration calorimetry (ITC).

EGCG and its analogs, (–)-epicatechin gallate (ECG), (–)-epigallocatechin (EGC) and (–)-gallocatechin gallate (GCG), are natural polyphenolic compounds extracted from green tea, and show little toxicity to human [12, 13]. The chemical structures of EGCG analogs are depicted in Fig. 1. It can be obviously found that GCG is the stereoisomer of EGCG. The structure of ECG is similar to EGCG but lacks the

3'-hydroxyl group on the trihydroxyl ring (B ring). The structure of EGC includes the 3'-hydroxyl group but lacks the gallate ester (D ring). Comparative analysis of EGC and EGCG allows an assessment of the gallate moiety role in inhibiting Aβ42 aggregation and remodeling Aβ42 mature fibrils. Similarly, comparative analysis of ECG and EGCG can address the role of 5-hydroxyl group on the trihydroxyl ring. And comparative analysis of GCG and EGCG can show the role of stereoisomer in the polyphenolic structure.

It has been demonstrated that the structural constraints and specific aromatic interactions directed polyphenol inhibitors to the amyloidogenic core [88]. Churches and co-workers [14] suggested that both the number of hydroxyl groups and the positioning of these groups on the polyphenolic structure are important against amyloid protein aggregation. Akaishi and co-workers [15] also demonstrated that phenolic hydroxyl groups were important for the inhibition of EGCG against Aβ42 aggregation. Many other researchers confirmed that galloyl moiety (D ring in Fig. 1) in polyphenols structure played an essential role of binding to many proteins [16-18]. In our previous work, we elucidated that epimers EGCG and GCG showed discrepancy inhibitory effects on lipase activity, indicating spatial conformation might have an important role of binding to protein [18].

These findings raise a challenge question of what link between the hydroxyl group, gallol moiety, and epimer in the polyphenolic structural analogs and corresponding anti-aggregatory activity. To meet the challenge, using EGCG, GCG, ECG, and EGC

analogs as model inhibitors, we would like to characterize the structure and activity between EGCG analogs and β-sheet linked polymerization and depolymerization of Aβ42 protein fibrils. Although EGCG and its structural analogs are well known to inhibit Aβ42 aggregation, however, it is not known the structural requirements by which EGCG analogs inhibit Aβ42 protein aggregation and remodel amyloid fibrils. Thus, we evaluate the effects of adding four polyphenolic structural analogs in each specific phase of fibrillation on Aβ42 aggregation and disaggregation. Therefore, three main purposes of this work are focused on: (1) to explore the influences of EGCG structural analogs on the Aβ42 aggregation/fibrillation when added in the lag and growth phases of Aβ42 fibrillation; (2) to address the effects of EGCG structural analogs on the Aβ42 disaggregation when adding in the equilibrium phase of Aβ42 fibrillation; (3) to evaluate the contribution efficiency of 3'-hydroxyl group, galloyl moiety, and epimer in EGCG structure on the redirection of Aβ42 amyloid formation. The findings of our work will shed light on the inhibitory mechanisms of EGCG analogs against Aβ42 aggregation, and provide the structured based mechanism between polyphenols inhibitors and Aβ42 amyloid protein at molecular level.

Materials and methods

Materials

Aβ42 with a purity of more than 95% was purchased from GL Biochem Ltd (Shanghai, China). Aβ42 protein was kept in -80 °C fringe before experimental usage. The polyphenols analogs of EGCG, ECG, EGC, and GCG with the purity of 98% were

bought from Shanghai Yuanye Biological Technology Co., Ltd (Shanghai, China). The molecular chemical structures of four EGCG analogs are shown in Fig. 1. Hexafluoroisopropanol (HFIP) with the purity of more than 99.5% was available from Sigma (St. Louis, MO, USA). All other chemicals and agents were of the analytic grades and bought from local sources in China.

r parameter determination

To facilitate the comparison of different EGCG analogs under various conditions, *r* representing the molar ratio of a certain EGCG analogs to Aβ42 was introduced in this work, which was calculated with Eq. (1):

$$r = \frac{[\text{EGCG analogs}]}{[\text{A}\beta 42]} \quad (1)$$

where: [EGCG analogs] and [Aβ42] are the final concentrations of each EGCG analog and Aβ42 (μmol/L) in phosphate buffer solutions (PBS) (pH 7.4), respectively.

The final Aβ42 concentration in PBS was 25 μmol/L, and the final concentrations of each EGCG analogs in PBS were 25, 125, and 250 μmol/L, respectively. Hence, in this work, the values of *r* were 1, 5, and 10, respectively. To maintain low oxygen partial pressure and suppress the oxidation of EGCG analogs, PBS was degassed for 20 min before use and the solutions were flushed with nitrogen during operations.

Aβ42 sample solution preparation

Lyophilized Aβ42 in the vial was stored at –80 °C fringe before use. The peptide was allowed to stand at room temperature for 30 min to avoid condensation upon

opening the vial cap. Aβ42 stock solution was prepared by dissolving the Aβ42 peptide in HFIP with the concentration of 1 mg/mL. The solution was subjected to ultrasonic concussion for 10 min and incubated at 25 ℃ for 30 min in order to eliminate all the secondary structures. Then the volatile solvent was removed off by vacuum freeze-drying overnight. The treated Aβ42 peptide was dissolved in 20 mmol/L NaOH solution with a concentration of 1 mg/mL. After ultrasonic concussion for 5 min, Aβ42 solution was centrifuged with the rate of 5,000 rpm for 5 min at 5 °C. 1 mL of supernatant was drawn and diluted with 100 mmol/L phosphate buffer solutions (PBS) (pH 7.4) to the final concentration of 25 μM Aβ42 for experiments.

Fibrillation kinetics monitoring by Thioflavin T (ThT) fluorescence

ThT fluorescence method was employed to monitor the fibrillation kinetics of Aβ42 in the absence and presence of EGCG analogs at different concentrations at 37 °C with the agitation of 200 rpm [19]. At appropriate intervals, aliquot of 200 μL samples was removed from the bulk solution and mixed with 2 mL of 20 μmol/L ThT. The solution was injected into a 1 cm-path length quartz cuvette and assayed on a Varian Cary Eclipse fluorescence spectrometer (Varian Inc., Palo Alto, California, USA). The excitation wavelength was 400 nm, and emission wavelength was 480 nm. The excitation and emission slits were both 5 nm. The scanning rate was 600nm/min and the resolution was 1.0 nm.

Analysis of kinetic parameters

Aβ42 fibrillation kinetic parameters were analyzed according to the method

reported by Wang and co-workers[20]. The fibrillation of Aβ42 could be described as a sigmoidal time-dependent curve which sequentially involves three stages, an initial lag phase where the ThT fluorescence intensity at 480 nm (I480) shows no changes, a subsequent fast growth phase where I480 increases exponentially with time, and a final equilibrium phase where I480 reaches a plateau indicating the end of fibril formation [21]. Hence, the I480 values were plotted as a function of incubation time and regressed by a sigmoidal curve described by Eq. (2):

$$Y = y_i + \frac{y_f}{1 + e^{-[(t-t_0)/\tau]}} \quad (2)$$

where Y is the I480, t is incubation time, t_0 is the time to 50% of maximal I480, and y_i, y_f, τ are all coefficients. Therefore, Aβ42 fibrillation kinetic parameters, the apparent rate constant for the growth of fibrils (k_{app}), the lag time (T_{lag}), and the I480 maximum (Y_{max}), can be derived from Eq. 2 and depicted as Eqs (3)-(5):

$$k_{app} = \frac{1}{\tau} \quad (3)$$

$$T_{lag} = t_0 - 2\tau \quad (4)$$

$$Y_{max} = y_f + y_i \quad (5)$$

Conformation analysis by circular dichroism (CD) spectroscopy

The secondary structure changes of Aβ42 protein during the fibrillation in the absence and presence of EGCG analogs were detected by a Jasco 810 circular dichroism spectrophotometer (Jasco Inc., Tokyo, Japan) according to the method in our previous work [22]. Specifically, an aliquot of 500 μL sample was taken out from the bulk solution at different incubation times and centrifuged at 5,000 rpm for 5 min. The

148 supernatant was injected into a 1-mm path length quartz cuvette. A background CD
149 spectrum of buffer solution was subtracted from the sample spectrum for baseline
150 correction. The conditions of CD analysis were: a resolution of 0.5 nm, scanning rate
151 of 100 nm/min, response time of 1 s, bandwidth of 2 nm, room temperature and the
152 wavelength ranges from 190 to 250 nm. The Aβ42 secondary elements of α-helix,
153 β-sheet, turn, and unordered coil were calculated from the spectra data using the
154 public database of DichroWeb (http://dichroweb.cryst.bbk.ac.uk/html/home.shtml)[23].
155 Deconvolution protocol: SELCON3. Specific parameters: file format of JASCO 1.50
156 (with preview); input and ourput units of theta; initial wavelenth of 250 nm; final
157 wavelength of 190 nm; optiional scaling factor of 1.0; mean residue weigh of 110.1
158 daltons (molecular weight / (number of residues -1)).

159 *Morphology detection by atomic force microscope (AFM)*

160 10 μL samples were pipetted onto freshly cleaved mica plate (1 cm × 1 cm) fixed
161 onto a glass slide and incubated at room temperature for 3 min. The remaining salts
162 and loose deposits in the suspension were triplicate rinsed with ultrapure water (50 μL,
163 Millipore) and then air-dried for a whole night. AFM images were obtained on a
164 dimension FastScan AFM (Bruker, German) with FASTSCAN-A probe in ScanAsyst
165 mode under ambient conditions. Scanning frequency was from 0.5 to 2.0 Hz. At least
166 three different regions of the surface were examined to verify that morphology was
167 similar throughout the sample [24]

Thermodynamic parameter (T_m) assessment by differential scanning calorimetry (DSC)

Thermodynamic parameter T_m, the transition midpoint temperature, was determined by a VP differential scanning calorimetry (MicroCal, Northampton, MA) [18]. Temperature scans were set from 30 to 90 °C at a scan rate of 1 °C/min (i.e., ca. 60 min for a round). The sample cell was loaded with Aβ42 solution in the absence or presence of a certain EGCG analogs, and the same concentration of PBS was loaded into the reference cell as the blank control. Samples were removed from the bulk solutions at a certain incubation time, which was set as the sampling time in Fig. 2D and 5. The samples and control were degassed for 15 min at 4 °C immediately before DSC scanning using the included degassing system. A buffer-buffer reference scan was subtracted from each sample scan prior to concentration normalization. DSC data were analyzed by MicroCal Origin Version 7.0 [18].

Inhibition and disaggregation of Protofibrils/Fibrils

Aβ42 solution alone was first pre-incubated at 37 °C with an agitation of 200 rpm for a certain time. At 10 h (the growth phase) and 24 h (the equilibrium phase), EGCG analogs were added into the preformed Aβ42 protofibril or fibril solutions with a final concentration of 125μmol/L (r=5) and further incubated to 40 h. At certain incubation times, aliquots of samples were removed from the bulk solution and examined by ThT fluorescence, CD spectroscopy, AFM, and DSC to evaluate the effect of EGCG analogs on the inhibition or disaggregation of Aβ42 protofibrils and fibrils.

Solubility measurement by bicinchoninic acid (BCA) protein assay

The inhibitory efficacy of EGCG analogs on Aβ42 aggregation and disaggregation was further studied by measuring the concentration of soluble Aβ42 in the supernatant with BCA protein assay [25]. Briefly, 20 μL of protein standards or Aβ42 samples were centrifuged at 12,000 rpm for 30 min, and then added to 220 μL of the mixture solutions of BCA reagent A and B (50:1, v/v, Beyotime Biotechnology Co., Shanghai, China). The mixed samples were subjected to a 96 well plate and incubated for 30 min at 37 °C. After that, the plate was cooling for 15 min at room temperature. The Aβ42 protein solubility was calculated by measuring the absorbance of each well on a Multiskan spectrum (Thermo Fisher Scientific Inc., MA, USA) at a wavelength of 562 nm.

Results and discussion

Fibrillation kinetics of Aβ42 alone

We first evaluated the fibrillation characteristics of Aβ42 alone from the aspects of kinetics, structure, morphology, and thermodynamics. The data were summarized in Fig. 2.

The Aβ42 fibrillation kinetics were assayed using ThT fluorescence due to the fact that the fibril contents can be quantified by ThT fluorescence intensity I480 [26]. As shown in Fig. 2A, Aβ42 fibrillation formation displayed a typical sigmoidal curve at physiological condition (37 °C and 100 mmol/L PBS). To obtain the kinetic parameters of Aβ42 fibrillation, the curve was fitted by Eq. (2) described by Nielsen

and co-workers [21], and T_{lag} value of 3.2±0.2 h, k_{app} value of 102.3±8.8 1/h, and Y_{max} value of 931.1±9.8 were achieved (Table 1). Accordingly, the sigmoidal time-course curve can be sequentially divided into three stages: a rate-limiting lag phase of 0-3.2 h (equal to the T_{lag} value) where an ordered oligomeric nucleus formed, a growth phase of 3.2-15 h (at 15 h, the ThT fluorescence intensity reached the maximum of 931.1±9.8) where Aβ42 protofibrils and fibrils formed/elongated with an apparent rate of 102.3±8.8 1/h, an equilibrium phase of >15 h where the mature fibrils formed and the fibril-mass concentration no longer changed [27-29].

The secondary structure changes of Aβ42 during fibrillation were detected by CD spectroscopy, and the spectra were fitted by the public database of DichroWeb [23]. The resulting Aβ42 secondary element percentages of α-helix, β-sheet, turn, and unordered coil were listed in Table S1. Since the fibrillation of Aβ42 mainly involves the conversion of β-sheet [27, 30], we presented the changing trend of β-sheet content during the fibrillation in Fig. 2B to facilitate the comprehensive analysis of different results. As listed in Table S1, the freshly prepared Aβ42 molecules (0 h) contained a random-coil content of 52.7% and a β-sheet content of 29.5%. The β-sheet contents increased rapidly at 0-3.2 h (the lag phase), indicating that most of the Aβ42 molecules converted into β-sheet rich nuclei and oligomers at this stage (Fig. 2B). With the further increase of incubation time at 3.2-15 h (the growth phase), the β-sheet structures gradually increased with time, which suggested the continued conversion of β-sheet rich oligomers from unfolded Aβ42 molecules and the

formation/elongation of protofibrils and fibrils from oligomers. However, after 15 h, the β-sheet structures started to decrease with incubation time. The same phenomenon has also been observed by Ruggeri et al. [27] during the study of impact of β-sheet content on the mechanical properties of Aβ42 fibrils. They suggested that the decrease of β-sheet content mainly stemmed from the sedimentation of insoluble aggregates during the measurement. In this study, since the kinetics of Aβ42 fibril formation have already reached the stationary equilibrium phase after incubation for 15 h according to the ThT signals (Fig. 2A), we also proposed that the reduction of β-sheet content resulted from the precipitation of insoluble aggregates during centrifugation before the CD assay (see the method section for detail information).

Fig. 2C shows the morphology images of Aβ42 fibrillation assayed by AFM. At 0 h, only a few early oligomers were observed due to the fact that Aβ42 mainly displayed as a random-coil monomer, which agreed well with the data of CD and ThT analysis. After 10 h incubation, abundant oligomers and protofibrils appeared in the image. At the end of growth phase (15 h), mature and un-branched Aβ42 fibrils were seen in the image. At an equilibrium phase of 24 h, branched fibrils with larger cross-sectional diameters were obviously found in AFM image. Although the fibril-mass concentration no longer changes at the equilibrium phase, the Aβ42 molecules were in a dynamic equilibrium, which led to secondary fibrillation on the basis of readily formed fibrils and therefore wider branched fibrils were formed [27, 28]. Our results were in well agreement with those reported in the literatures that the surfaces of Aβ42

fibrils could serve as templates for the replication of the parent structure, which resulted in the form of wider branched fibrils [31, 32].

Furthermore, DSC was employed to investigate the transition midpoint temperature (T_m) of Aβ42 during the fibrillation process. Fig. 2D showed the T_m values picked from the DSC spectra. It showed that Aβ42 fibrillation could be divided into three distinct phases according to T_m values. At 0-8 h, the 1st phase, T_{m1} value decreased with the incubation time from 55 to 50°C, indicating that the thermostability of Aβ42 declined. Within this period, Aβ42 formed nuclei and oligomers according to the ThT intensity and AFM image (Fig. 2A and C). Since the formation of nuclei and oligomers were reversed and unstable, the T_{m1} value declined. At 10-18 h (the 2nd phase), another transition midpoint temperature, T_{m2}, showed up and remained a constant value of 70 °C within this stage. It suggested that more stable species were formed in the solution. According to the AFM image in Fig. 2C, these stable species might be long and un-branched Aβ42protofibrils/fibrils. At 20-30 h, T_{m1} and T_{m2} merged into T_{m3} and gradually increased from 60 to 67 °C. The merge of T_{m1} and T_{m2} indicated that most of the nuclei, oligomers, and protofibrils have formed relatively homogeneous fibrils at this stage. Moreover, the increase of T_{m3} value at 20-24 h were assigned to the secondary fibrillation and the formation of more stable and wider branched fibrils described in AFM images (Fig. 2C, 24 h).

Effects of EGCG analogs on Aβ42 fibrillation when added in the lag phase

As above mentioned, the Aβ42 alone fibrillation kinetics displayed a typical

sigmoidal curve, which can be sequentially divided into three stages: lag phase, fast growth phase and equilibrium phase. By adding EGCG analogs in the lag phase, the influences of four EGCG analogs on Aβ42 fibrillation were investigated and the results were depicted in Fig. 3. It can be obviously found that ThT intensity decreased with the increasing of concentrations from 25, 125, to 250 μmol/L (r=1, 5, and 10) for each EGCG analogs. The 50% inhibition concentration (*IC50*) values for EGCG, GCG, ECG and EGC were 1.70±0.17, 2.92±0.22, 4.27±0.26, 18.37±2.17 μmol/L, respectively (Seen Fig. S1). It suggested that EGCG analogs show capabilities of inhibiting Aβ42 fibrillation. The ThT experimental data were regressed by Eq. (2) and the kinetic parameters were summarized in Table 1. T_{lag} values were prolonged while k_{app} and Y_{max} values decreased in a concentration-dependent manner through adding the four EGCG analogs in the lag phase. Therefore, from Table 1 and Fig. S1, we confirmed that the inhibitory effects of the four EGCG analogs decreased by the order of EGCG ≈ GCG > ECG > EGC.

The β-sheet contents of Aβ42 alone increased firstly at 0-15 h and then decreased at 15-36 h (Fig. 4A, black line). When EGCG analogs were added into the Aβ42 solution in the initial lag phase, the contents of β-sheet changed to different extents for each analog (Fig. 4A and Table S1). In view of EGCG and GCG, the β-sheet contents firstly increased before 3.2 h, and then dramatically decreased to 15.5 and 17.2% after 24-h incubation, respectively. By comparing the profiles for EGCG and GCG in Fig. 4A, it can also be found that the inhibitory effect of GCG was better than EGCG before ca.

10 h, indicating that GCG had better capability for prolonging the lag time of Aβ42. This conclusion was in consistence with T_{lag} values in Table 1, where T_{lag} value for GCG at r=1 (9.4 h) was much longer than those for EGCG (4.8 h), ECG (3.7 h), and EGC (5.6 h). As for ECG and EGC, the turning points of the profiles were about 11 and 15 h, and the β-sheet contents at 36 h were 26.1 and 32.1%, respectively. Summarily, the inhibitory effects of the four molecules decreased in the order of EGCG>GCG>ECG>EGC.

To address the thermostability of EGCG analogs and Aβ42 combination, the effects of EGCG analogs on the DSC curves of Aβ42 were investigated when EGCG analogs were added in the lag phase. Fig. 5A showed that the addition of EGCG analogs broadened the peak width of Aβ42 by the order of GCG > EGCG > ECG > EGC, indicating that they bound to Aβ42 nonspecifically and broke its homogeneity to some extents. Noticeably, the T_m value for GCG was the highest, which suggested that GCG and Aβ42 nuclei formed more stable complexes in the lag phase, prolonging the lag time and preventing the oligomerization and fibrillation. This phenomenon was in well agreement with the T_{lag} value in Table 1 and CD results in Fig. 4A.

The morphology of Aβ42 aggregates with EGCG analogs added in the lag phase were detected through AFM after 24 h co-incubation (Fig. 6). Compared with the AFM images of Aβ42 alone in Fig. 2C (24 h), amorphous aggregates, instead of fibrils, appeared at the equilibrium stage with the addition of the four EGCG analogs, revealing that the four EGCG analogs could prevent the formation of fibrils. However,

the size of the aggregates for EGCG and GCG were much larger than those for EGC and ECG, which was in consistence with Y_{max} values in Table 1. This phenomenon might stem from the fact that ThT mainly binds to the cavities running parallel to the fibril axis of Aβ42 which is rich in β-sheet structure, rather than amorphous aggregates or monomers whose β-sheet contents were low [24, 28]. The results, however, implied that EGCG and GCG could remodel Aβ42 into ThT undetectable, off-pathway aggregates, which were also found by other researchers [5, 33].

Effects of EGCG analogs on Aβ42 inhibition when added in the growth phase

To evaluate whether EGCG analogs can inhibit the aggregation of Aβ42 when added in the growth phase, Aβ42 was incubated alone for 10 h and then EGCG analogs were added to the solution with a final concentration of 125 μmol/L (r=5). As can be seen in Fig. 7A, after the addition of the four analogs, the ThT intensity decreased by the order of EGCG ≈ GCG > ECG > EGC, indicating that the four EGCG analogs inhibited the Aβ42 oligomers and protofibrils and the inhibitory effects decreased by the order of EGCG ≈ GCG > ECG > EGC. AFM images in Fig. 7B confirmed that average size of the aggregates for EGCG and GCG was smaller than that of Aβ42 alone (Fig. 2C, 10 h), suggesting that EGCG and GCG could inhibit the formation of oligomers and protofibrils. However, there were also some amorphous aggregates with sizes larger than those of Aβ42 alone (Fig. 2C, 10 h). Since the ThT intensity and CD signal were both weak at this point (Figs. 7A and 4B), it could be inferred that the large amorphous aggregates resulted from the remodel of

unfolded or partially unfolded oligomers by EGCG or GCG [5, 33]. As for ECG and EGC, the remodel were not observed since the size of the aggregates in Fig. 7B were smaller than those of Aβ42 alone (Fig. 2C, 10 h).

Furthermore, as can be observed from Fig. 4B, when adding four EGCG analogs in the growth phase of fibrillation, the β-sheet contents of the Aβ42 peptide started to decrease instead of increase, indicating that the four EGCG analogs could bind to oligomers and protofibrils, unfold them, and prevent the fibrillation process (Fig. 4B). At the fast growth phase, Aβ42 alone showed broad peak width and two T_m values (Figs. 5B and 2), indicating that oligomers and protofibrils co-existed. The addition of EGCG analogs merged the two T_m values and narrow the peak width (Fig. 5B), suggesting that the homogeneity was increased by the analogs. Taken together, it implied that the EGCG analogs inhibited the conversion of protofibrils from oligomers and therefore increased the homogeneity of the solution.

Effects of EGCG analogs on remodeling Aβ42 fibrillation when added in the equilibrium phase

In order to investigate whether EGCG analogs remodeled mature Aβ42 fibrils, Aβ42 was incubated alone for 24 h and then EGCG analogs were added to the solution with a final concentration of 125 μmol/L (r=5). As shown in Fig. 8A, ThT intensity decreased with the addition of EGCG analogs by the order of EGCG > GCG > ECG > EGC. At about 35 h, ThT intensity became unchanged. AFM images in Fig. 8B showed that the morphology of Aβ42 converted from fibrils to small

357 oligomers, indicating that all the four EGCG analogs can disaggregate Aβ42 fibrils.
358 Specifically, the sizes of aggregates for EGCG and GCG were larger than those for
359 ECG an EGC, again indicating that EGCG and GCG can remodel the small oligomers
360 to amorphous aggregates [5, 33].

361 From the β-sheet contents variances of Aβ42 in the absence and presence of
362 EGCG analogs (Fig. 4C), when EGCG analogs were added in the equilibrium phase,
363 as shown in Fig. 4C, the β-sheet contents started to increase and then decrease with
364 increasing of incubation time. It suggested that EGCG analogs first disaggregated
365 fibrils and released soluble β-sheet-containing monomers/oligomers in the solution
366 (resulting in the increase of β-sheet contents), and then unfolded or partially unfolded
367 these monomers/oligomers (resulting in the decrease of β-sheet contents). The T_{m3}
368 value of Aβ42 alone at equilibrium phase of 24 h was 67 °C (Fig. 2D). The addition of
369 EGCG, GCG, ECG, and EGC decreased the T_{m3} value to 56.51±0.10, 57.37±0.12,
370 58.25±0.08, and 61.27±0.19 ℃, respectively (Fig. 5C). Since the typical temperature
371 of Aβ42 alone at lag phase was about 50-55 °C (Fig. 2D), close to the above four
372 temperatures, it can be inferred that the four EGCG analogs remodeled the fibrils into
373 oligomers and the disaggregation effects were by the order of
374 EGCG>GCG>ECG>EGC.

375 *Molecular interaction mechanism between EGCG analogs and Aβ42 protein*

376 In this study, molecular interactions between four EGCG analogs and Aβ42 were
377 investigated by adding the EGCG analogs at the lag phase, growth phase, and

equilibrium phase of Aβ42 fibrillation. EGCG analogs could inhibit the fibrillation of Aβ42 and disaggregate the preformed fibrils and protofibrils in dependence on structural characteristics. Among the four EGCG analogs, EGCG and GCG could remodel the Aβ42 fibrils into ThT undetectable, off-pathway amorphous aggregates no matter added in each phase. To further confirm the results, we detected the solubility of Aβ42 in the absence or presence of EGCG analogs when added in different phases. As shown in Fig. 9, the solubility of Aβ42 in the presence of EGCG analogs was higher than Aβ42 alone for the three fibrillation phases with or without ultrasonic treatment, and the Aβ42 solubility increased by the order of EGC < GCG ≈ EGCG < ECG. Obviously, EGC showed the least Aβ42 solubility, which indicated the worst inhibitory effect. As for EGCG and GCG, the solubility was lower than ECG, it was probably that the two molecules remodeled the disaggregated oligomers into amorphous aggregates. Similarly, Ehrnhoefer and co-workers [5] found that EGCG directly bound to unfolded Aβ42 molecules and redirected them into unstructured, off-pathway oligomers. Palhano and co-workers [9] observed that EGCG remodeled the fibrils of Aβ40 into amorphous aggregates. Wang and co-workers [34] also demonstrated that EGCG can bind to insulin, another amyloid protein, change its secondary structure, and induce it into amorphous aggregates.

In order to probe the molecular interaction mechanisms between the four EGCG analogs and Aβ42, we further determined the half maximal inhibitory concentration (IC_{50}) of the four EGCG analogs by varying the addition concentration from 0 to 250

399 μmol/L. It was found that the IC_{50} value for EGCG, GCG, ECG, and EGC were
400 1.70±0.17, 2.92±0.22, 4.27±0.26, and 18.37±2.17 μmol/L, respectively (Fig. S1).
401 Taken together, we found that EGCG showed the best inhibitory effect, followed by
402 GCG, ECG, and EGC (Figs. 3, 6, 4B and Table 1). In view of the structural
403 characteristics of four molecules (Fig. 1), EGCG and GCG are epimers, comparative
404 analysis of GCG and EGCG can discover the role of stereoisomer on Aβ42 fibrillation
405 in the polyphenolic structure. EGCG was better than GCG in the aspects of IC_{50}, k_{app},
406 and Y_{max}, while GCG was better than EGCG according to T_{lag} (Table 1). This
407 phenomenon might stem from the difference ways EGCG and GCG bound to Aβ42
408 molecules. Similar results were observed our previous work [18]. We found that epimers
409 EGCG and GCG bound with protein in different way. For instance, in the solution
410 state, some EGCG molecules directly bound to proteins and others just encountered
411 proteins collisionally, while all GCG molecules only bound to proteins. Moreover, the
412 binding constant of EGCG to proteins was much higher than that of GCG [18]. These
413 results indicated that spatial conformation of EGCG and GCG caused different
414 binding mode with protein, leading to different inhibitory effects. Nevertheless,
415 spatial conformation of EGCG and GCG did not change the remodel ability from
416 disaggregated Aβ42 oligomers into amorphous aggregates (Figs. 6, 7 and 8).

417 The structural difference between EGCG and ECG lies on 3'-hydroxyl group.
418 Comparative analysis of ECG and EGCG can address the role of 3'-hydroxyl group
419 on the trihydroxyl ring (B ring). From IC_{50} values in Fig. S1 and kinetic parameters in

Table 1, it indicated that 3'-hydroxyl group was an important functional group for the inhibition of Aβ42 fibrillation. This phenomenon was also confirmed by Akaishi and co-workers, who studied structural requirements for the flavonoid fisetin in inhibiting fibril formation of Aβ protein, and suggested that 3', 4'-dihydroxyl group, but not 3- or 7-hydroxyl group, is essential for the inhibitory effect of fisetin on Aβ1-42 fibril formation [15]. According to our previous work and literature, the interaction between hydroxyl group and Aβ42 is supposed to be hydrogen bonding [5, 11, 35]. Lacking 3'-hydroxyl group would decline the binding affinity of ECG to Aβ42, and suppress the remodel ability of Aβ42 (Figs. 6, 7, and 8).

The structure of EGC lacks the gallate ester (D ring) in comparison with EGCG. Comparative analysis of EGC and EGCG allowed an assessment of the gallate moiety role in inhibiting Aβ42 aggregation and remodeling Aβ42 mature fibrils. From IC_{50} in Fig. S1 and kinetic parameters in Table 1, it is reasonably speculated that the galloyl moiety played an essential role in the inhibition of Aβ42 fibrillation. The galloyl moiety contains one phenyl group and three hydroxyl groups, so it could bind to Aβ42 through hydrophobic interactions and hydrogen bonding. Lacking galloyl moiety greatly lowered the binding affinity to Aβ42, EGC showed the least influence on the conformation and thermostability of Aβ42 (Figs. 4 and 5). Ishii and co-workers [36] compared the interactions between human serum albumin (HSA) and EGCG as well as EGC. The authors pointed out that the galloyl moiety was of critical importance in the interaction between EGCG and HAS [33].

Therefore, it was first demonstrated the structural characteristics of EGCG to inhibit amyloid Aβ42 aggregation and remodel amyloid fibers. In other words, 3'-hydroxyl group, gallol moiety and epimer of these functional groups in the EGCG structure were all important to inhibit amyloid fibrillation, and the inhibitory effect decreased by the order of galloyl moiety > 3'-hydroxyl group > epimer.

Conclusions

To elucidate the structural characteristics of EGCG inhibiting amyloid Aβ42 aggregation and remodeling amyloid fibers, molecular interactions between four EGCG analogs and Aβ42 were investigated by ThT fluorescence, CD spectroscopy, AFM, DSC and BCA protein assay. Results showed that four EGCG analogs could prevent the increase of β-sheet structure of Aβ42 and inhibit Aβ42 fibrillation when added at the lag and growth phases. When added at the equilibrium phase, EGCG analogs remodeled the preformed protofibrils and fibrils to oligomers and unfolded or partially unfolded the oligomers from β-sheet. From the Aβ42 solubility measurement, EGCG and GCG could remodel the fibrils into ThT undetectable, off-pathway amorphous aggregates. The inhibitory effects of the EGCG analogs were EGCG > GCG > ECG > EGC. Comprehensive analysis of functional groups of EGCG analogs, the contribution efficiency of those main groups decreased by the order of galloyl moiety > 3'-hydroxyl group > epimer to inhibit Aβ42 fibrillation. In conclusion, this work provided the structural characteristics of EGCG analogs on inhibiting Aβ42 fibrillation at molecular level.

Acknowledgements

This work was financially supported by the project of Beijing Municipal Natural Science Foundation (5142013). AFM experiments are supporting by the long-term subsidy mechanism from the Ministry of Finance and the Ministry of Education of China.

References

1. M. Goedert and M. G. Spillantini, *Science*, 2006, **314**, 777-781.

2. T.-I. Kam, Y. Gwon and Y.-K. Jung, *Cell Mol Life Sci*, 2014, **71**, 4803-4813.

3. P. Joshi, E. Turola, A. Ruiz, A. Bergami, D. Libera, L. Benussi, P. Giussani, G. Magnani, G. Comi and G. Legname, *Cell Death Differ*, 2014, **21**, 582-593.

4. N. J. Izzo, J. Xu, C. Zeng, M. J. Kirk, K. Mozzoni, C. Silky, C. Rehak, R. Yurko, G. Look and G. Rishton, *PloS one*, 2014, **9**, e111899.

5. D. E. Ehrnhoefer, J. Bieschke, A. Boeddrich, M. Herbst, L. Masino, R. Lurz, S. Engemann, A. Pastore and E. E. Wanker, *Nat Struct Mol Biol*, 2008, **15**, 558-566.

6. K. Rezai-Zadeh, G. W. Arendash, H. Y. Hou, F. Fernandez, M. Jensen, M. Runfeldt, R. D. Shytle and J. Tan, *Brain Res*, 2008, **1214**, 177-187.

7. K. Rezai-Zadeh, D. Shytle, G. Arendash, N. Sun, H. Hou, J. Zeng, T. Mori, D. Morgan and J. Tan, *Cell Transplant*, 2007, **16**, 342-342.

8. Y. Porat, A. Abramowitz and E. Gazit, *Chem Biol Drug Des*, 2006, **67**, 27-37.

9. F. L. Palhano, J. Lee, N. P. Grimster and J. W. Kelly, *J Am Chem Soc*, 2013, **135**, 7503-7510.

10. A. Smith, B. Giunta, P. C. Bickford, M. Fountain, J. Tan and R. D. Shytle, *Int J Pharm*, 2010, **389**, 207-212.

11. S. Wang, X.-Y. Dong and Y. Sun, *J Phys Chem B*, 2012, **116**, 5803-5809.

12. S. Mandel, O. Weinreb, T. Amit and M. B. H. Youdim, *J Neurochem*, 2004, **88**, 1555-1569.

13. Y. Levites, T. Amit, M. B. Youdim and S. Mandel, *J Biol Chem*, 2002, **277**, 30574-30580.

14. Q. I. Churches, J. Caine, K. Cavanagh, V. C. Epa, L. Waddington, C. E. Tranberg, A. G. Meyer, J. N. Varghese, V. Streltsov and P. J. Duggan, *Bioorg Med Chem Lett*, 2014, **24**, 3108-3112.

15. T. Akaishi, T. Morimoto, M. Shibao, S. Watanabe, K. Sakai-Kato, N. Utsunomiya-Tate and K. Abe, *Neurosci Lett*, 2008, **444**, 280-285.

16. M. Nakai, Y. Fukui, S. Asami, Y. Toyoda-Ono, T. Iwashita, H. Shibata, T. Mitsunaga, F. Hashimoto and Y. Kiso, *J Agr Food Chem*, 2005, **53**, 4593-4598.

17. N. Popovych, J. R. Brender, R. Soong, S. Vivekanandan, K. Hartman, V. Basrur, P. M. Macdonald and A. Ramamoorthy, *J Phys Chem B*, 2012, **116**, 3650-3658.

18. S. Wang, Z. Sun, S. Dong, Y. Liu and Y. Liu, *PLoS ONE*, 2014, **9**, e111143.

19. K. J. Barnham, V. B. Kenche, G. D. Ciccotosto, D. P. Smith, D. J. Tew, X. Liu, K. Perez, G. A. Cranston, T. J. Johanssen and I. Volitakis, *Proc Natl Acad Sci U S A*, 2008, **105**, 6813-6818.

20. S. Wang, X.-Y. Dong and Y. Sun, *Biochem Eng J*, 2012, **63**, 38-49.

21. L. Nielsen, R. Khurana, A. Coats, S. Frokjaer, J. Brange, S. Vyas, V. N. Uversky and A. L. Fink, *Biochemistry*, 2001, **40**, 6036-6046.

22. S. Wang, S. Dong, R. Zhang, H. Shao and Y. Liu, *Process Biochem*, 2014, **49**, 237-243.

509 23. DichroWeb. Available: http://dichroweb.cryst.bbk.ac.uk/html/home.shtml
510 Accessed 2015 June 15.
511 24. J. Zhang, X. Zhou, Q. Yu, L. Yang, D. Sun, Y. Zhou and J. Liu, *ACS Appl*
512 *Mater Interfaces*, 2014, **6**, 8475-8487.
513 25. X. Wang, X. Wang, C. Zhang, Y. Jiao and Z. Guo, *Chemical Science*, 2012, **3**,
514 1304-1312.
515 26. H. LeVine, *Method Enzymol*, 1999, **309**, 274-284.
516 27. F. S. Ruggeri, J. Adamcik, J. S. Jeong, H. A. Lashuel, R. Mezzenga and G.
517 Dietler, *Angew Chem Int Edit*, 2015.
518 28. R. Sabaté, M. Gallardo and J. Estelrich, *Int J Biol Macromol*, 2005, **35**, 9-13.
519 29. A. Lomakin, D. S. Chung, G. B. Benedek, D. A. Kirschner and D. B. Teplow,
520 *Proc Natl Acad Sci U S A*, 1996, **93**, 1125-1129.
521 30. T. Lührs, C. Ritter, M. Adrian, D. Riek-Loher, B. Bohrmann, H. Döbeli, D.
522 Schubert and R. Riek, *Proc Natl Acad Sci*, 2005, **102**, 17342-17347.
523 31. J. S. Jeong, A. Ansaloni, R. Mezzenga, H. A. Lashuel and G. Dietler, *J Mol*
524 *Biol*, 2013, **425**, 1765-1781.
525 32. M. Žganec and E. Žerovnik, *Biochimica et Biophysica Acta (BBA) - General*
526 *Subjects*, 2014, **1840**, 2944-2952.
527 33. J. Bieschke, J. Russ, R. P. Friedrich, D. E. Ehrnhoefer, H. Wobst, K.
528 Neugebauer and E. E. Wanker, *Proc Natl Acad Sci U S A*, 2010, **107**, 7710-7715.
529 34. S. Wang, X.-Y. Dong and Y. Sun, *Int J Biol Macromol*, 2012, **50**, 1229-1237.

35. S. Wang, F.-F. Liu, X.-Y. Dong and Y. Sun, *J Phys Chem B*, 2010, **114**, 11576-11583.

36. T. Ishii, T. Ichikawa, K. Minoda, K. Kusaka, S. Ito, Y. Suzuki, M. Akagawa, K. Mochizuki, T. Goda and T. Nakayama, *Biosci Biotechn Biochem*, 2010, **75**, 100-106.

Figure Legends

Fig. 1 Chemical structures of EGCG analogs. GCG is the stereoisomer of EGCG. The structure of ECG lacks the 5-hydroxyl group on the trihydroxyl ring (B ring). The structure of EGC lacks the gallate ester (D ring).

Fig. 2 Fibrillation process of Aβ42 alone in PBS (pH 7.4) at 37 °C for 0-36 h at the concentration of 25 μmol/L. A: kinetics of Aβ42 fibrillation by ThT fluorescence; B: changes of β-sheet contents by CD spectra; C: morphologies by AFM images; D: transition midpoint temperature (T_m) by DSC.

Fig. 3 Effects of EGCG analogs on the fibrillation kinetics of Aβ42 when added in the lag phase. The concentration of Aβ42 was 25 μmol/L. The concentrations of EGCG analogs can be calculated from the [EGCG analogs]/[Aβ42] ratio, which were 25, 125, and 250 μmol/L. Experiments were carried out in 100 mmol/L PBS (pH7.4) at 37°C.

Fig. 4 Effects of EGCG analogs on the secondary structure changes of Aβ42 when added at different phases of Aβ42 fibrillation. A: lag phase (0 h); B: growth phase (10 h); C: equilibrium phase (24 h). The concentrations of Aβ42 and EGCG analogs were 25 μmol/L and 125 μmol/L (r=5), respectively. Experiments were carried out in 100 mmol/L PBS (pH7.4) at 37°C.

Fig. 5 Effects of EGCG analogs on the thermodynamic parameter (T_m) of Aβ42 when added at different phases of Aβ42 fibrillation. A: lag phase (0 h); B: growth phase (10 h); C: equilibrium phase (24 h). The concentrations of Aβ42 and EGCG analogs were 25 μmol/L and 125 μmol/L (r=5), respectively.

559 Fig. 6 Effects of EGCG analogs on the morphology of Aβ42 aggregates when added
560 at the lag phase. The concentrations of Aβ42 and EGCG analogs were 25 μmol/L and
561 125 μmol/L (r=5), respectively. Images were taken after 24 h incubation in 100
562 mmol/L PBS (pH7.4) at 37°C.
563 Fig. 7 Effects of EGCG analogs on the kinetics (A) and morphology (B) of Aβ42
564 when added at the growth phase of 10 h. The concentrations of Aβ42 and EGCG
565 analogs were 25 μmol/L and 125 μmol/L (r=5), respectively. AFM images were taken
566 after 14 h addition of EGCG analogs.
567 Fig. 8 Effects of EGCG analogs on the kinetics (A) and morphology (B) of Aβ42
568 aggregates when added at the equilibrium phase of 24 h. The concentrations of Aβ42
569 and EGCG analogs were 25 μmol/L and 125 μmol/L (r=5), respectively. AFM images
570 were taken after 16 h addition of EGCG analogs.
571 Fig. 9 Effects of EGCG analogs on Aβ42 solubility when added at different phases of
572 Aβ42 fibrillation. A: lag phase (0 h); B: growth phase (10 h); C: equilibrium phase (24
573 h). The concentrations of Aβ42 and EGCG analogs were 25 μmol/L and 125 μmol/L
574 (r=5), respectively.
575 Fig. S1 IC_{50} values of EGCG analogs. The concentrations of Aβ42 was 25 μmol/L.
576
577

578

579 **Table 1.** Effects of EGCG analogs on the kinetic parameters of Aβ42

580 fibrillation/aggregation.

	r=[EGCG analogs] /[Aβ42]	T_{lag} (h)	k_{app} (1/h)	Y_{max}
0 (Aβ42 alone)		3.2±0.2	102.3±8.8	931.1±9.8
EGCG	1	4.8±0.4	27.4±1.0	263.9±3.5
	5	NA*	NA*	75.9±6.0
	10	NA*	NA*	64.0±5.9
GCG	1	9.4±0.3	49.3±2.1	277.9±3.2
	5	NA*	NA*	72.7±5.2
	10	NA*	NA*	55.4±5.4
ECG	1	3.7±0.4	19.8±0.7	282.7±5.8
	5	19.9±1.0	10.6±0.2	175.8±12.3
	10	26.3±1.6	7.2±0.4	159.1±9.3
EGC	1	5.6±0.5	50.2±1.6	441.6±23.3
	5	6.2±0.3	34.3±2.0	291.5±6.4
	10	6.4±0.6	30.9±2.4	259.7±3.8

581 *NA: Data were unavailable due to the low Y_{max}.

582

583

584 **Fig. 1**

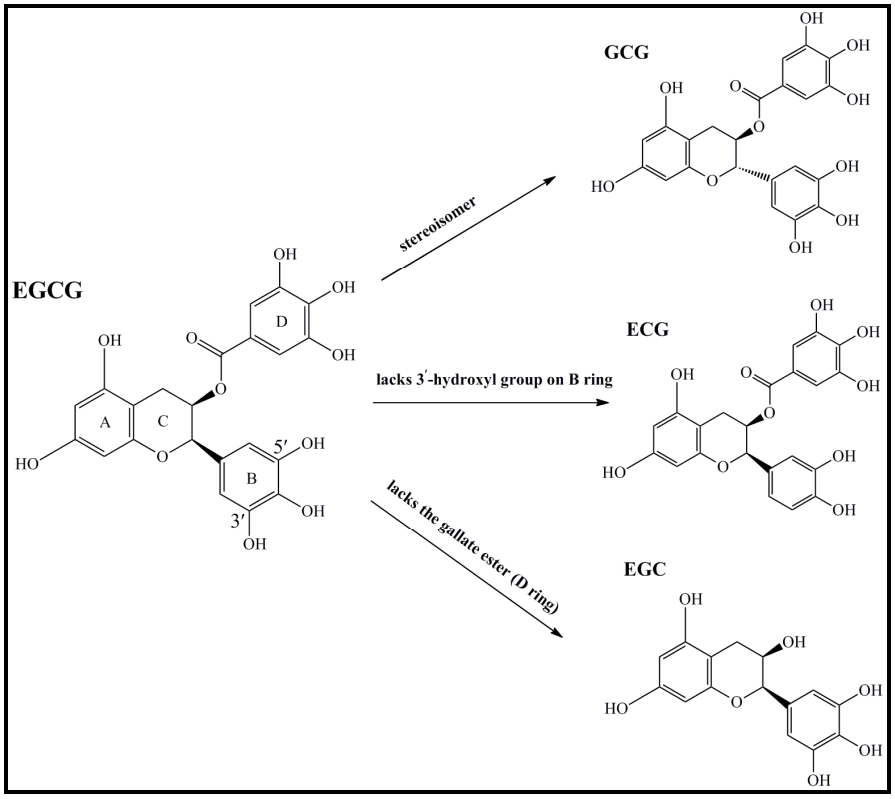

585

586

587

588 **Fig. 2**

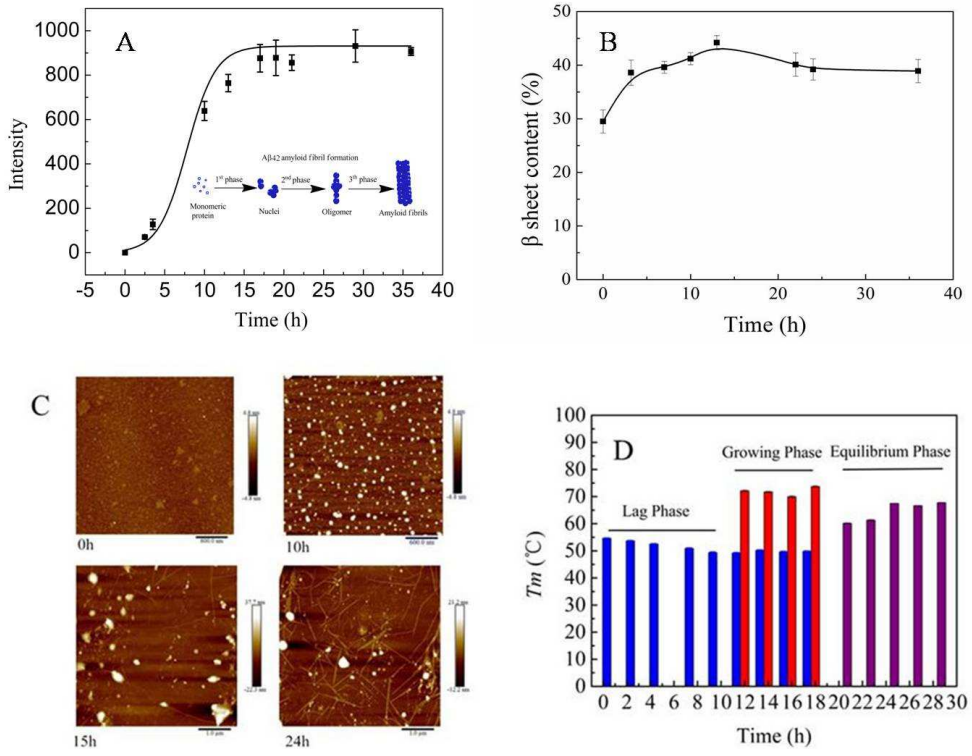

589

590

591 **Fig. 3**

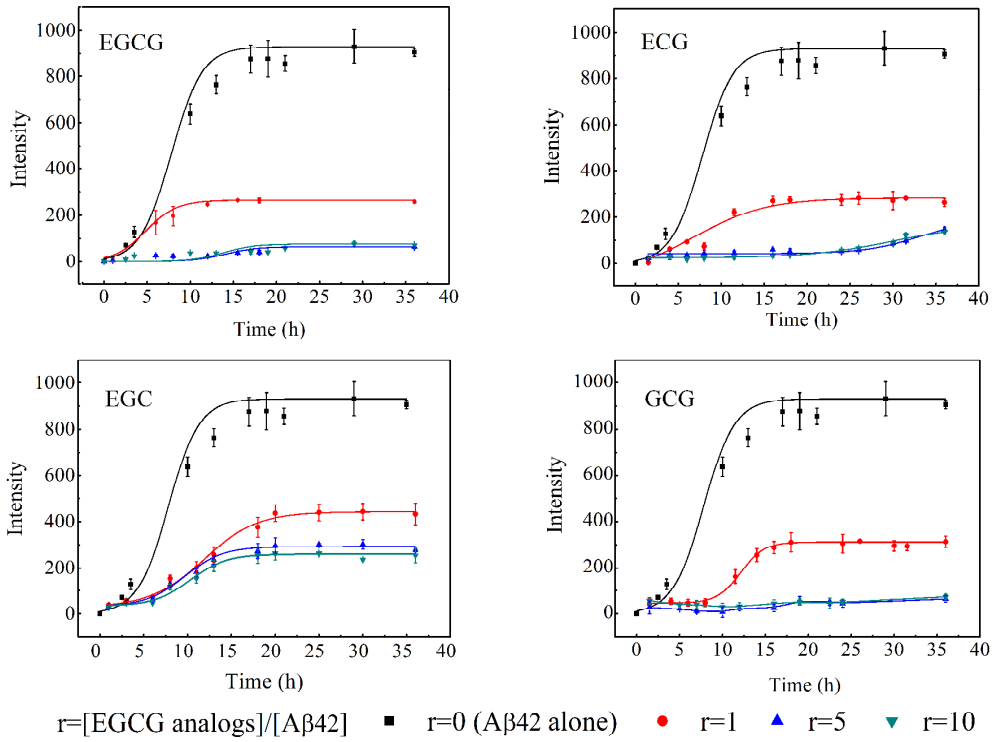

592

593

594 **Fig. 4**

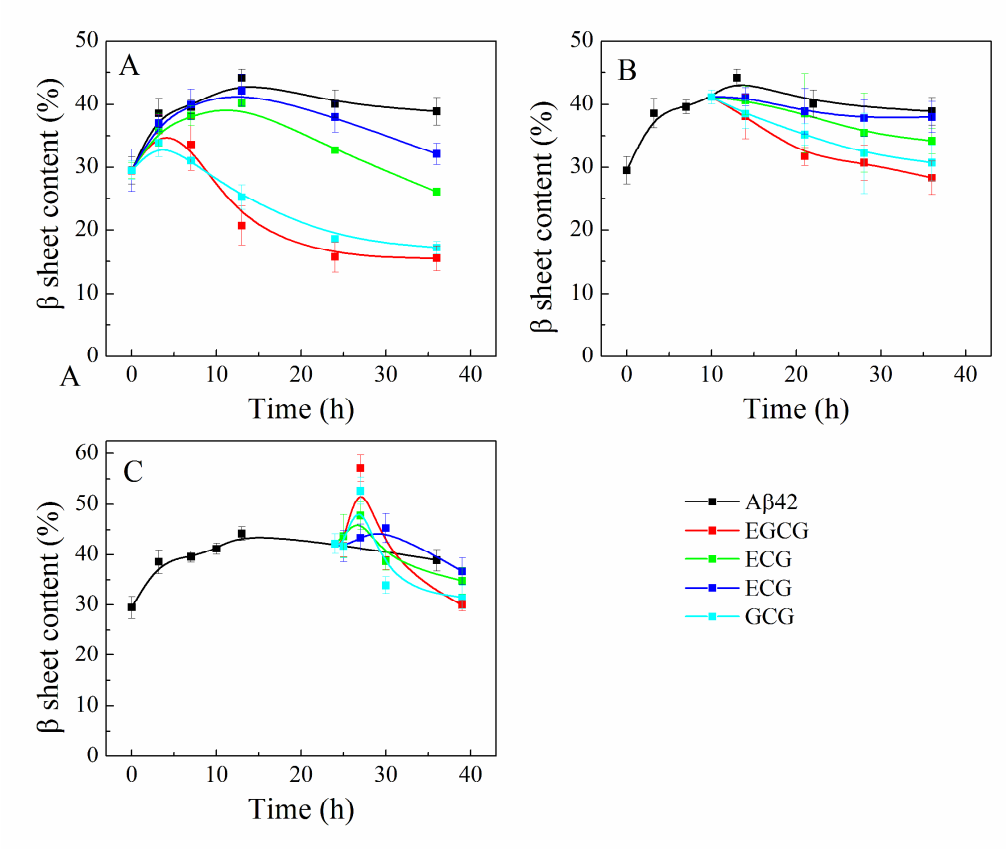

595

596

597 **Fig. 5**

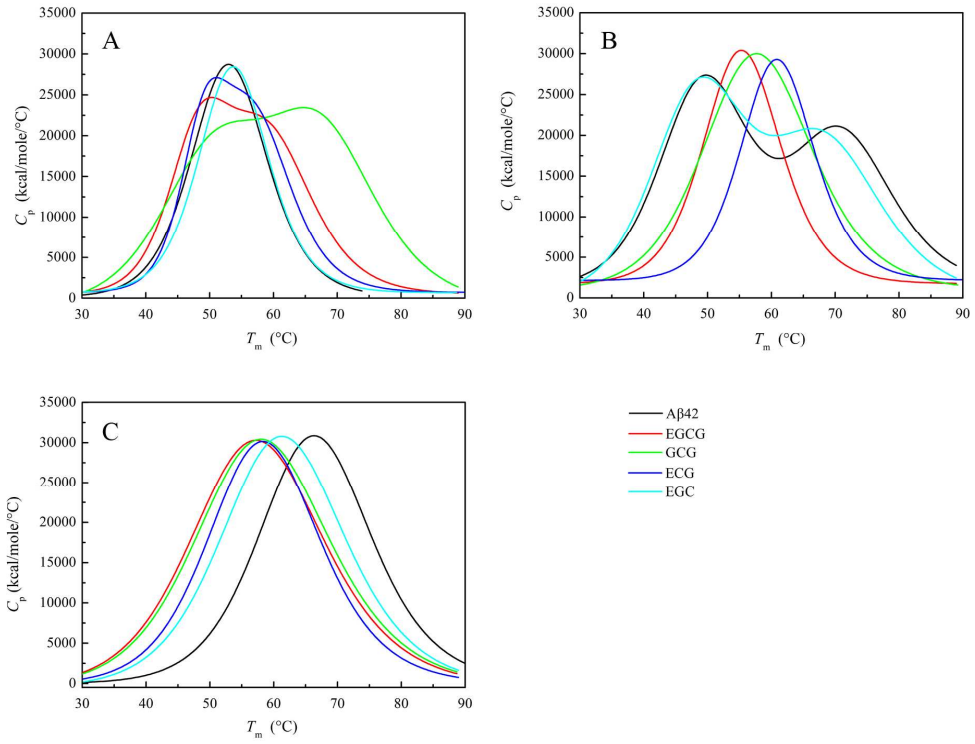

598

599 **Fig. 6**

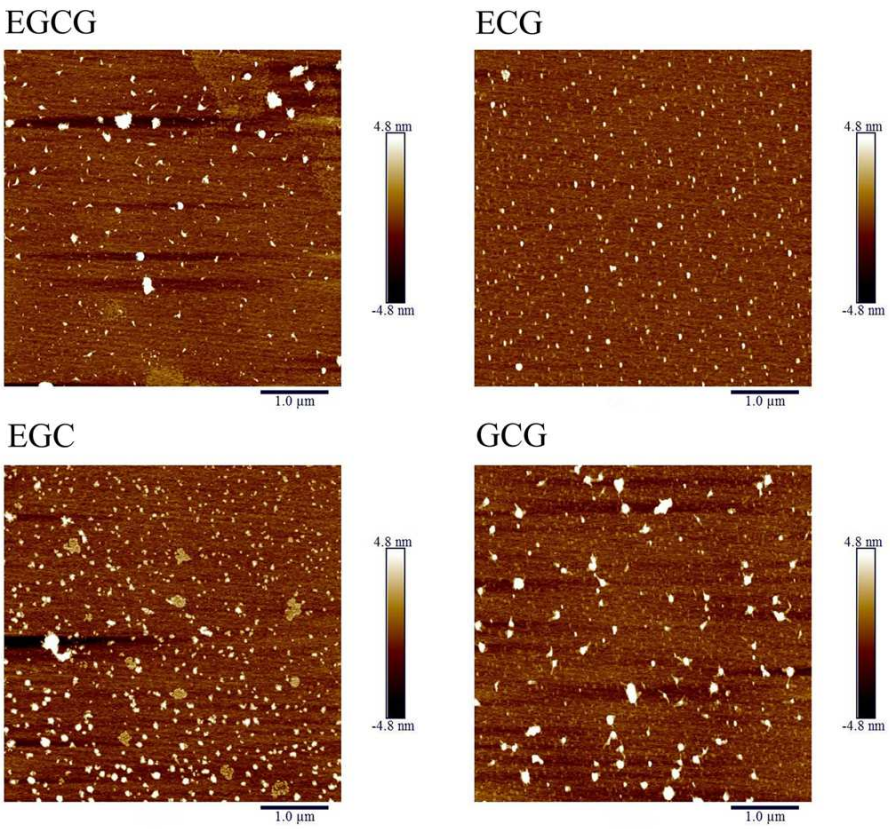

600

601

602 **Fig. 7**

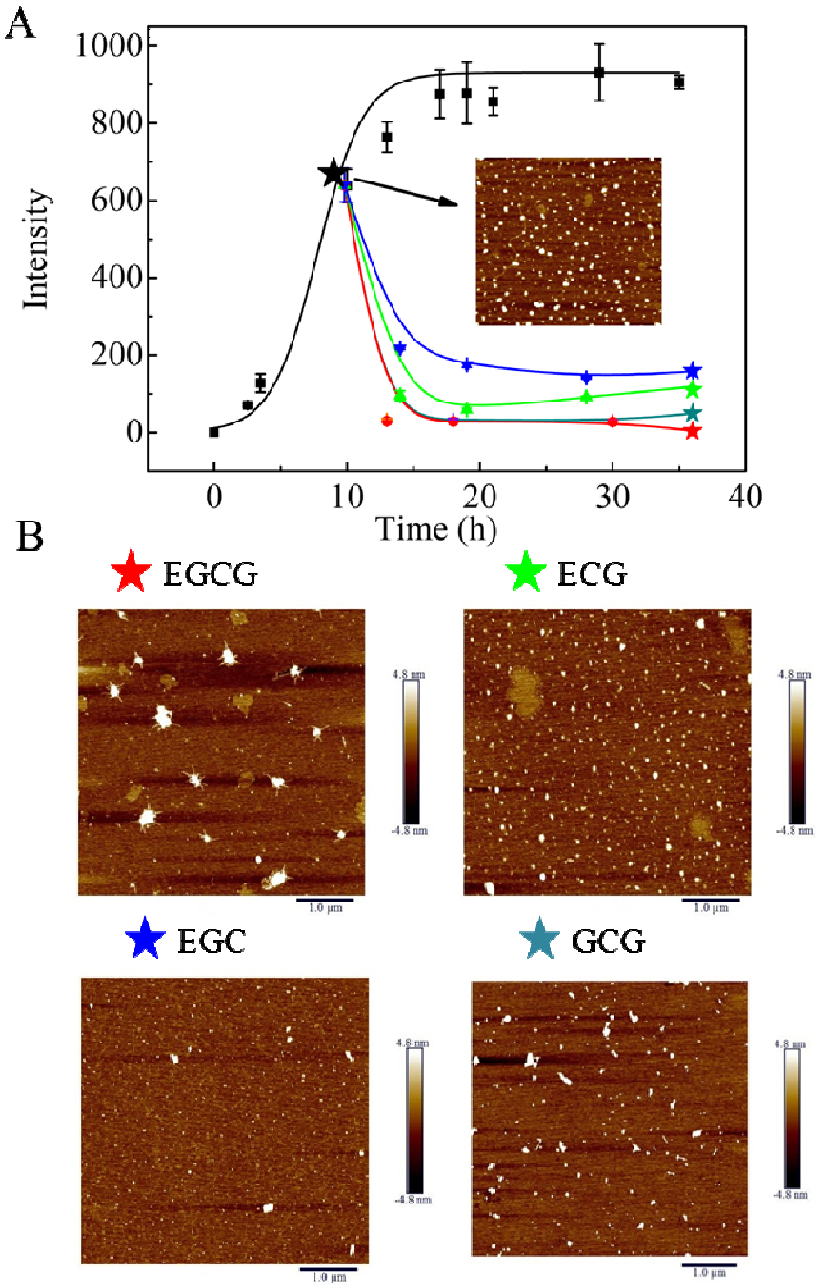

603

604

605 **Fig. 8**

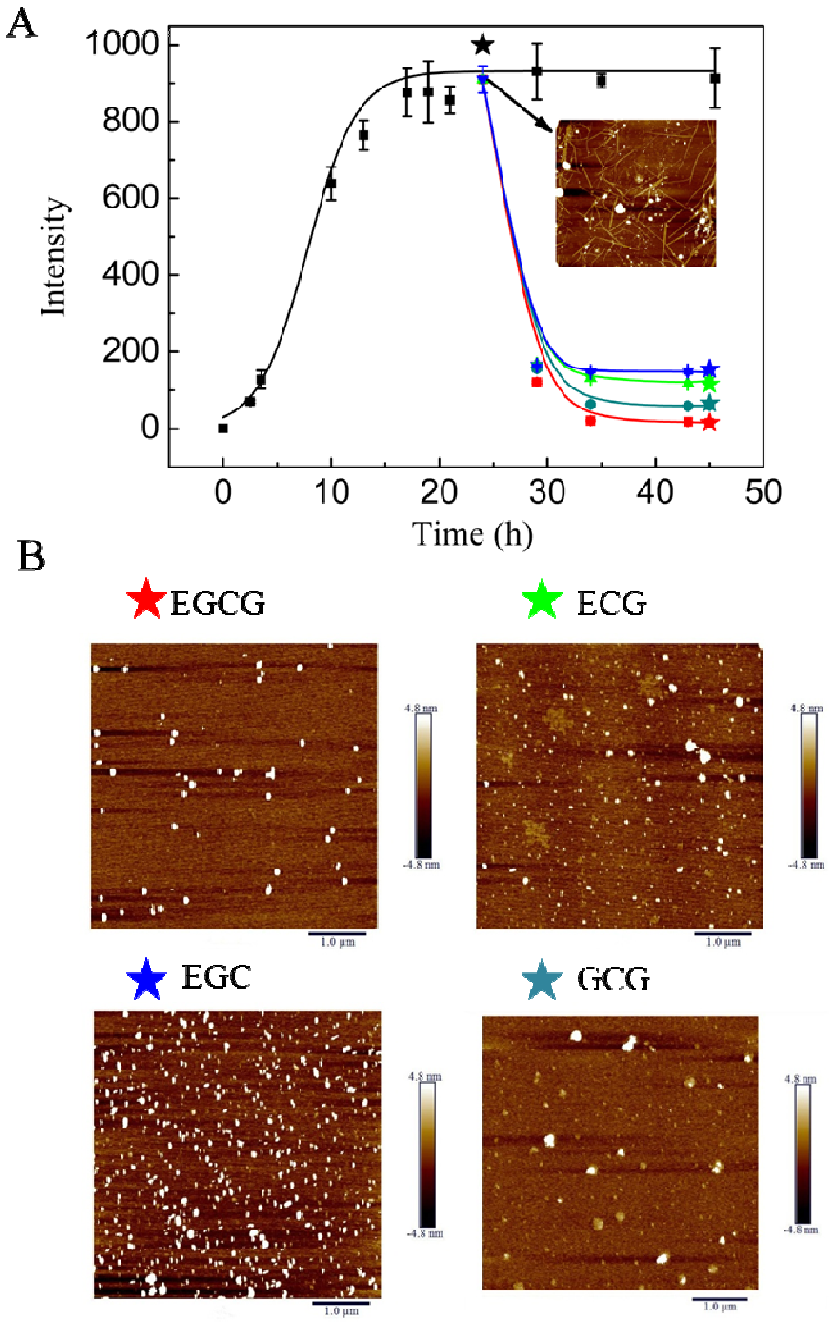

606

607

608

609

610 **Fig. 9**

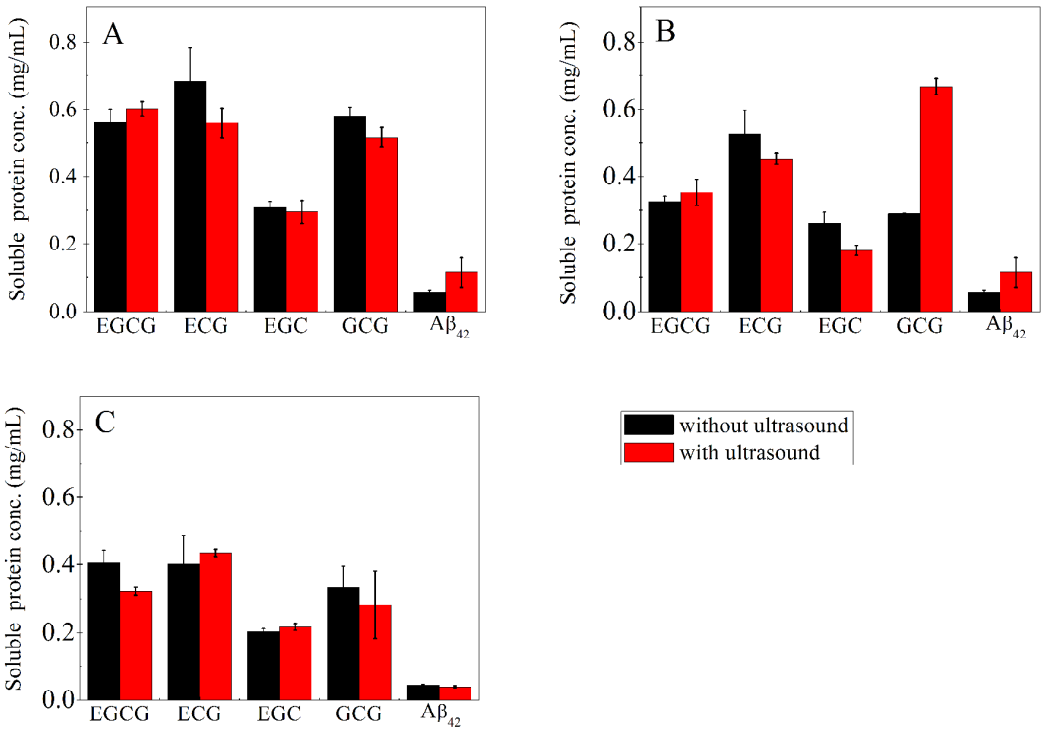

611

612